Acta Pharmaceutica Sinica B 2023;13(5):2124–2137

Chinese Pharmaceutical Association
Institute of Materia Medica, Chinese Academy of Medical Sciences

Acta Pharmaceutica Sinica B

www.elsevier.com/locate/apsb
www.sciencedirect.com

ORIGINAL ARTICLE

Novel STING-targeted PET radiotracer for alert and therapeutic evaluation of acute lung injury

Duo Xu[a,b,c,†], Fan Yang[b,c,†], Jiayao Chen[a,c,†], Tianxing Zhu[b,c], Fen Wang[d], Yitai Xiao[b,c], Zibin Liang[c], Lei Bi[c], Guolong Huang[c], Zebo Jiang[b,c,*], Hong Shan[a,c,*], Dan Li[b,c,*]

[a]*Center for Interventional Medicine, the Fifth Affiliated Hospital, Sun Yat-sen University, Zhuhai 519000, China*
[b]*Department of Nuclear Medicine, the Fifth Affiliated Hospital, Sun Yat-sen University, Zhuhai 519000, China*
[c]*Guangdong Provincial Key Laboratory of Biomedical Imaging and Guangdong Provincial Engineering Research Center of Molecular Imaging, the Fifth Affiliated Hospital, Sun Yat-sen University, Zhuhai 519000, China*
[d]*Department of Pathology, the First Affiliated Hospital, Sun Yat-sen University, Guangzhou 510080, China*

Received 20 September 2022; received in revised form 11 December 2022; accepted 15 December 2022

KEY WORDS

Acute lung injury (ALI);
Stimulator of interferon genes (STING);
PET imaging;
[^{18}F]FBTA

Abstract Acute lung injury (ALI), as a common clinical emergency, is pulmonary edema and diffuse lung infiltration caused by inflammation. The lack of non-invasive alert strategy, resulting in failure to carry out preventive treatment, means high mortality and poor prognosis. Stimulator of interferon genes (STING) is a key molecular biomarker of innate immunity in response to inflammation, but there is still a lack of STING-targeted strategy. In this study, a novel STING-targeted PET tracer, [^{18}F]FBTA, was labeled with high radiochemical yield (79.7 ± 4.3%) and molar activity (32.5 ± 2.9 GBq/μmol). We confirmed that [^{18}F]FBTA has a strong STING binding affinity (K_d = 26.86 ± 6.79 nmol/L) and can be used for PET imaging in ALI mice to alert early lung inflammation and to assess the efficacy of drug therapy. Our STING-targeted strategy also reveals that [^{18}F]FBTA can trace ALI before reaching the computed tomography (CT) diagnostic criteria, and demonstrates its better specificity and distribution than [^{18}F]fluorodeoxyglucose ([^{18}F]FDG).

*Corresponding authors.
E-mail addresses: jiangzb5@mail.sysu.edu.cn (Zebo Jiang), shanhong@mail.sysu.edu.cn (Hong Shan), lidan25@mail.sysu.edu.cn (Dan Li).
[†]These authors made equal contributions to this work.

Peer review under the responsibility of Chinese Pharmaceutical Association and Institute of Materia Medica, Chinese Academy of Medical Sciences.

https://doi.org/10.1016/j.apsb.2022.12.017

1. Introduction

Acute lung injury (ALI) is the cause of respiratory failure and is characterized by acute lung inflammation accompanied by tissue damage, immune cell infiltration, increased endothelial permeability, pulmonary edema, and gas interchange disturbance[1]. ALI, often occurring in the case of pneumonia, sepsis, aspiration of gastric contents, or severe trauma, is present in about 10% of intensive care unit (ICU) patients worldwide, and the mortality rate is as high as 30%−40%[2−4]. In addition, respiratory failure caused by ALI is also a secondary symptom of advanced coronavirus disease 2019 (COVID-19) infection, and has become a major clinical challenge for the treatment[5,6]. Alert diagnosis and preventive drug intervention, before patients reach the diagnostic criteria of ALI, have aroused research interest due to the reduced mortality and improved prognosis[7].

Molecular changes, an early event of ALI, are earlier than pathological changes. However, the currently used clinical diagnostic methods such as chest X-ray and computed tomography (CT) imaging are mainly based on pathological changes, the late events that occur after inflammatory cells and fluid accumulate in lungs, which are not helpful for the alert diagnosis of ALI[8−10]. For alert diagnosis, the lung injury prediction score (LIPS) and early acute lung injury (EALI) score based on clinical data (including susceptibility risk factors, comorbidities, and acute physiological variables) and radiographic imaging (including chest X-ray and CT imaging) have been used to predict ALI in high-risk patients, but it has been confirmed that the negative predictive values of both LIPS and EALI scores are too high to guide treatment[8,11,12]. Improper or delayed ALI treatment, caused by the lack of effective alert diagnostic strategies, has increased the mortality of patients[13]. Once the diagnosis is delayed, only symptomatic treatment can be done, such as aspirin, corticosteroid and β2-agonist[7,14]. A molecular targeting strategy that allows both alert diagnosis of ALI and its response to treatment is therefore needed.

Positron emission tomography (PET) imaging, providing key information about early molecular changes in disease, treatment response and prognosis, is an ideal method to achieve non-invasive molecular level alert diagnosis and therapeutic evaluation of ALI[15,16]. Among the various PET tracers, [^{18}F]fluorodeoxyglucose ([^{18}F]FDG) can trace ALI through enhanced glucose metabolism of active immune cells[17]. However, the limited specificity, high non-specific heart uptake and false-positive findings prevent the use of [^{18}F]FDG in ALI diagnosis[13,18,19]. Targeting immune cells and their biomarkers can provide greater specificity for functional status during ALI. The lactoferrin, CD11b, chemokine (C−C motif) ligand type 2 (CCR2) and the very late antigen-4 (VLA-4) have been used as biomarkers for imaging lung inflammation[20−24]. However, lactoferrin has limited specificity as an inflammatory target, mainly since lactoferrin is a secreted protein widely distributed in various tissues and their secretions[20]. The lactoferrin-targeted probe ^{67}Ga/^{68}Ga-citrate is mainly distributed in the blood pool, which affects the judgment of lung injury lesions[20,21]. Similarly, CD11b is expressed on several types of myeloid cells and some non-myeloid cells, and CD11b-targeted probe ^{64}Cu-αCD11b has a high non-specific uptake in bones and is unfavorable for the identification of lung lesions[22]. The CCR2 targeted probe ^{64}Cu-DOTA-ECL1i has a fast blood clearance rate, leading to insufficient radioactivity enrichment in the lesions and limited detection sensitivity[23]. In addition, VLA-4-targeted probe ^{64}Cu-LLP2A and all the ^{64}Cu-labeled probes mentioned above need to be imaged at 24 h post-injection[22−24], which leads to delays in the diagnosis of acute lung inflammation and the increased radiological protection space and time costs. Inadequacies of biomarkers and probes prompt us to develop a new alternative molecular targeting strategy for ALI imaging.

As a crucial adapter of the innate immune system, the STING pathway is implicated in the pathogenesis of several diseases, including ALI[25−27]. During lung injury caused by pathogens stimulation, DNA fragments leaked from damaged lung tissues activate the cyclic guanosine monophosphate-adenosine synthase (cGAS)-STING pathway, leading to the production and release of inflammatory cytokines that regulate the immune system response to pathogens stimulation[25,26,28]. Increasing clinical evidence has also shown that STING is a pivotal protein in the early pathological progression of ALI, and represents the molecular basis for immune cell activation and recruitment. All of these implicate STING as a sensitive and specific inflammatory biomarker during ALI. Therefore, we conceived that targeting STING for molecular-level imaging could enable alert and therapeutic evaluation of ALI.

Given the report of STING as an important biomarker of ALI, we set out to develop a novel STING-targeted PET tracer ([^{18}F]FBTA) to test our hypothesis. [^{18}F]FBTA was constructed using a high affinity STING agonist-benzothiophene derivative previously reported[29], which can non-invasively and specifically monitor the expression of STING in lung injury lesions for ALI alert and therapeutic evaluation. In addition, we confirm that [^{18}F]FBTA can detect small ALI lesions earlier than CT, and demonstrate that STING-targeted probe has better specificity and distribution than [^{18}F]FDG.

2. Results

2.1. Preparation and characterization of [^{18}F]FBTA

The labeling precursor (compound **5**) and non-radioactive reference ([^{19}F]FBTA) were synthesized using the previously published methods[29−31], and details are shown in Supporting Information Fig. S1. ^{1}H-NMR and ^{13}C-NMR spectrum of all compounds are shown in Supporting Information Figs. S2−S6. The two-steps radiolabeling routes of [^{18}F]FBTA are presented in Fig. 1a. High-performance liquid chromatography (HPLC) analysis in Fig. 1b showed that the retention times of [^{19}F]FBTA and [^{18}F]FBTA were 16.96 and 17.20 min, respectively, and the similar retention time confirmed that [^{18}F]FBTA was successfully radiolabeled with ^{18}F. The decay-corrected radiochemical yields of [^{18}F]FBTA was 79.7 ± 4.3% (n = 3) with a whole radio-synthesis time was about 40 min. The radiochemical purity of [^{18}F]FBTA was more than 99% after HPLC purification (Supporting Information Fig. S7) and the molar activity was calculated as 32.5 ± 2.9 GBq/μmol (n = 3) from the UV standard curve (Supporting Information Fig. S8). The octanol-to-water partition coefficient (log$P$) of [^{18}F]FBTA is 0.73 ± 0.10, indicating that the tracer is a lipophilic compound. As shown in Supporting Information Fig. S9, [^{18}F]FBTA exhibits good stability in saline and ethanol.

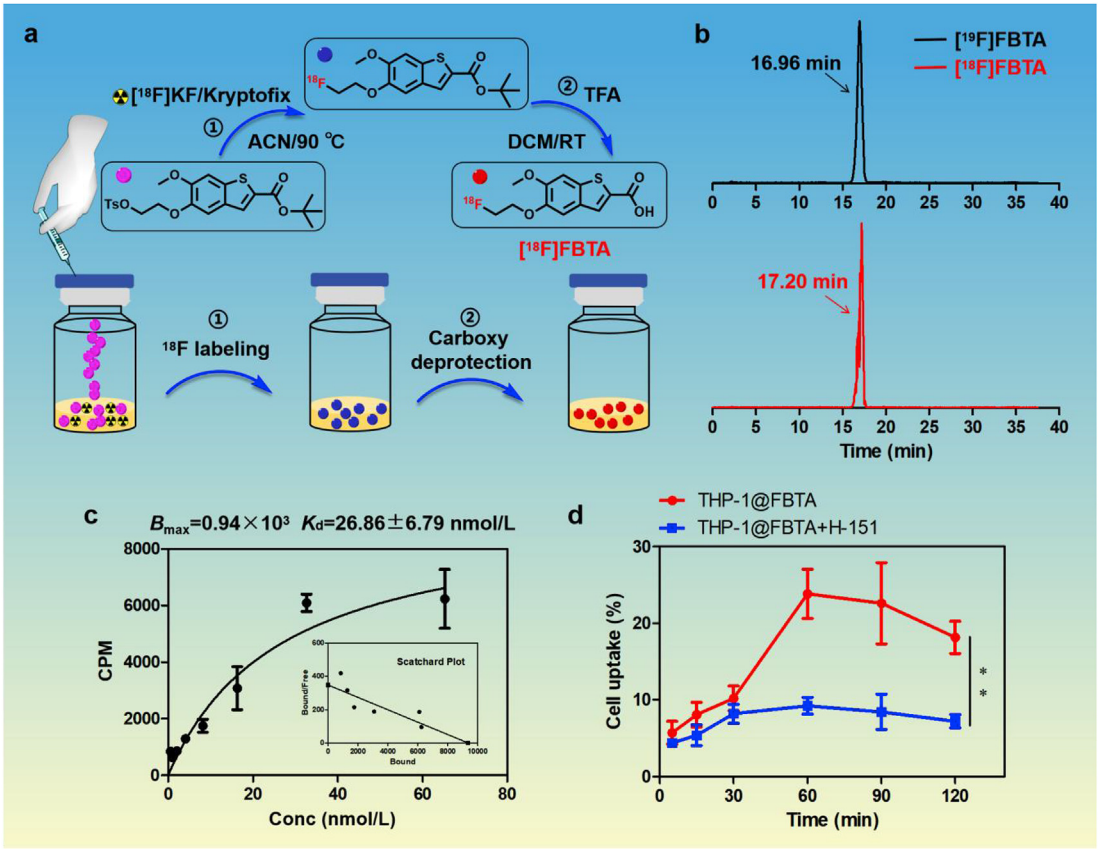

Figure 1 Radiolabeling and STING binding affinity of [^{18}F]FBTA. (a) The radiolabeling routes of [^{18}F]FBTA. (b) HPLC chromatograms of [^{18}F]FBTA (in red) and its non-radioactive compound [^{19}F]FBTA (in black). (c) Saturation binding assay of [^{18}F]FBTA in THP-1 cell lines. (d) The radioactivity uptake varies with incubation time in THP-1 cells with or without the addition of the STING inhibitor H-151. The data are shown as mean ± SD (n = 3). $^{**}P < 0.01$.

The saturation curve of [^{18}F]FBTA in THP-1 cells is shown in Fig. 1c. From this curve, the receptor binding affinity value (K_d) was calculated as 26.86 ± 6.79 nmol/L, and the maximum number of binding sites (B_{max}) was 0.94 × 10^3 per cell. To validate the binding specificity of the STING-targeted probe, cell-specific binding assay was performed. As shown in Fig. 1d, the uptake of [^{18}F]FBTA in THP-1 cells reached 23.83 ± 2.88% after 1 h-incubation and could be inhibited obviously by STING inhibitor H-151 (9.23 ± 0.98%, $^{**}P < 0.01$), indicating that [^{18}F]FBTA is a STING-binding radioligand and has high specificity and selectivity for targeting STING *in vitro*.

2.2. *PET imaging of STING to accurately quantify and alert of ALI*

To confirm that the STING-targeted probe can accurately quantify the ALI lesions, mice with varying degrees of ALI were used for [^{18}F]FBTA-PET imaging. In these experiments, a novel STING-targeted probe was first used to diagnose ALI *in vivo*. Compared with the control group, the ALI mice had a significant radioactive accumulation in lung lesions, and the more severe the ALI, the higher the radioactive enrichment (Fig. 2 and Table 1). The radioactive uptake values were expressed as percentage injected dose per gram (%ID/g). The uptake of lung lesions (15.96 ± 0.62 %ID/g) and lung to muscle ratio (10.62 ± 2.67) reached the maximum in the ALI-24 h group (mice inhaled with lipopolysaccharide (LPS) for 24 h). Mice in ALI-12 h group were also co-injected with [^{19}F]FBTA (50 μg per mouse) and [^{18}F]FBTA (11.1−14.8 MBq) to verify the specificity of the tracer. The PET images and data (Supporting Information Fig. S10 and Table S3) showed that the [^{19}F]FBTA blocked group had lower lung lesions uptakes (2.16 ± 0.33 %ID/g) and lower lung to muscle ratio (1.51 ± 0.26) when compared with the ALI group (6.33 ± 0.32 %ID/g, 4.77 ± 0.16, $^{***}P < 0.001$), indicating high *in vivo* specificity of [^{18}F]FBTA to STING. CT images showed no qualitative difference between the control group and the ALI-2 h group (mice inhaled with LPS for 2 h), but PET images, acquired 1 h after [^{18}F]FBTA injection, showed significant qualitative difference in the lungs of mice between saline group and the ALI-2 h group ($^{***}P < 0.001$, Table 1 and Supporting Information Fig. S11). Indeed, significant accumulation was seen in the lungs of ALI mice due to the high affinity and specificity of the radiotracer for STING.

As shown in Fig. 2, Supporting Information Fig. S12, Fig. S13 and Table S2, there is a large amount of radioactive enrichment in the kidneys and intestines, and a certain amount of radioactive uptake in the liver at 1 h p.i., which is mainly due to the non-specific uptake caused by metabolism of [^{18}F]FBTA. The uptake of [^{18}F]FBTA in the heart is relatively low at 1 h p.i., which will help to judge the inflammatory lesions in the lungs. Data from PET images (Fig. 2b and c and Supporting Information Table S1) and biodistribution studies (Fig. 2d) also show increased uptake in

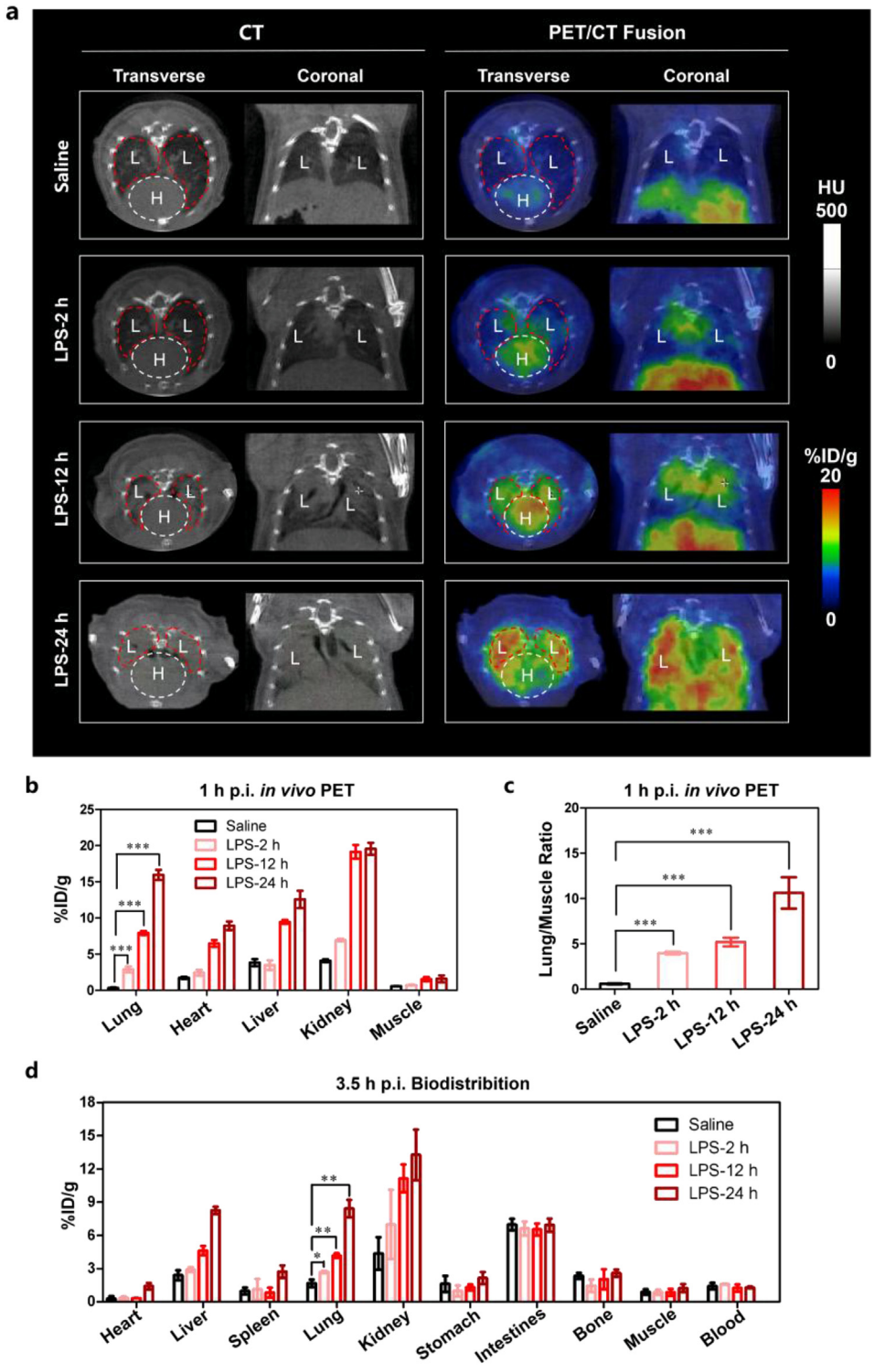

Figure 2 [^{18}F]FBTA-PET imaging, quantification and biodistribution in ALI mice with different degrees. (a) Transverse and coronal PET/CT images of [^{18}F]FBTA (11.1−14.8 MBq) in saline-inhaled mice (control group) and LPS-induced mice for 2, 12 and 24 h (ALI groups). The lungs are indicated by red lines and hearts are indicated by white lines. L presents lung and H presents heart. (b) Quantification of [^{18}F]FBTA accumulation in the lung, heart, liver, kidney and muscle at 1 h p.i. PET data are shown as percent injected dose per gram (%ID/g) ± SD ($n = 3$). (c) Lung to muscle ratios of control group and ALI groups derived from PET quantification. (d) Biodistribution data of [^{18}F]FBTA in major organs of control group and ALI groups at 3.5 h p.i. Data are shown as %ID/g ± SD ($n = 3$). *$P < 0.05$, **$P < 0.01$ and ***$P < 0.001$.

the heart, liver, and kidney with the extension of LPS induction time, indicating that the long-time LPS induction may cause systemic inflammatory response.

2.3. The distribution of STING in the lungs of ALI mice and its relationship with the uptake value of PET imaging

To realize the full functions of PET and improve clinical decision-making, ideally, the distribution and quantification of image-derived biomarkers *in vivo* should be consistent with the histology-derived biomarkers *in vitro*. Mice inhaled with LPS through the nasal cavity and induced for 2, 12, and 24 h, respectively, were expressed as ALI-2 h, ALI-12 h, and ALI-24 h group. Mice inhaled with saline in the nasal cavity served as controls. H&E and STING immunohistochemical staining revealed increased inflammatory cells and STING expression in all LPS-induced mice compared with the control group and a statistically significant increase in the expression of STING following LPS-treated time prolonged (Fig. 3a). Notably, the PET-derived uptake values (%ID/g) of lung lesions have strong correlations with H&E score ($r^2 = 0.8669$) and STING immunohistochemical score ($r^2 = 0.8189$) of lungs, respectively (Fig. 3b and c). Western blot results also showed that the expression of STING was significantly high in these LPS-induced lungs of ALI mice, which was consistent with STING immunohistochemical staining (Fig. 3d).

The strong infiltration of neutrophils, monocytes and macrophages in the lung is the key pathological process of ALI[32,33]. To confirm STING-positive ($STING^+$) cell types during ALI, flow cytometry sorting was performed in the lungs of ALI mice. Consistently, flow cytometry data showed the frequency and number of macrophages and neutrophils were increased in the lungs of LPS-induced ALI mice, compared with the control group ($^{***}P < 0.001$, Fig. 3e). More interestingly, we also found that the frequency and number of $STING^+$ macrophages and $STING^+$ neutrophils in lungs of ALI mice were significantly increased ($^{***}P < 0.001$, Fig. 3f). In addition, the results also showed that the frequency and number of $STING^+$ dendritic cells (DC), $STING^+$ $CD8^+$ $CD3^+$ T cells and $STING^+$ $CD4^+$ $CD3^+$ T cells were largely unchanged in the control group and ALI group (Supporting Information Fig. S14a, b).

Consistent with the results of H&E and STING immunohistochemical in mice, we found that STING was also highly expressed in human lung inflammatory tissues, while lowly expressed in healthy human lung tissues ($^{***}P < 0.001$, Fig. 3g). These results demonstrate the possibility of future studies on human ALI using the STING-targeted probe.

2.4. The comparison of STING targeting strategy and [^{18}F]FDG-PET imaging in ALI mice

[^{18}F]FDG can trace inflammation by active glucose metabolism, and has been used to image lung inflammation in humans[19,34,35]. [^{18}F]FDG-PET imaging of ALI mice was also performed for comparison. PET-derived quantification at 1 h p.i. demonstrated an approximately 2.7-folds increase in the [^{18}F]FBTA *versus* [^{18}F]FDG in lungs of ALI mice (15.96 ± 0.62 *vs*. 5.82 ± 1.59 %ID/g, $^{***}P < 0.001$) (Fig. 4a and b and Table 1). In addition, [^{18}F]FBTA had lower non-specific uptake in hearts (8.92 ± 0.53 %ID/g) and higher lung to heart ratios (1.79 ± 0.05) compared with [^{18}F]FDG (29.50 ± 4.84 %ID/g, 0.20 ± 0.04) at 1 h p.i. (Fig. 4b and c and Table S1). Biodistribution experiments are more likely to reflect more accurate probe distribution without blood interference. The *ex vivo* biodistribution studies of [^{18}F]FBTA and [^{18}F]FDG at 3.5 h p.i. are almost consistent with the PET imaging results at 1 h p.i. (Fig. 4d).

2.5. In vivo PET imaging and ex vivo quantification of STING to evaluate treatment of ALI

In previous studies, aspirin showed the potential to reduce LPS-induced pulmonary inflammation in human[7]. To determine whether our STING-targeted strategy could be applied to the therapeutic evaluation of ALI and the STING specificity of the probe, the PET-derived quantification, histology staining and flow cytometry analysis in lungs of ALI mice in response to treatment with aspirin were investigated. At 1 h p.i., the PET-derived radioactive uptake values and lung to muscle ratios of ALI mice treated with aspirin were much lower than saline-treated group ($^{***}P < 0.001$ and $^{**}P < 0.01$, respectively, Fig. 5a–c, and Table 1). The results of PET imaging at 1 h p.i and *ex vivo* biodistribution study at 3.5 h p.i. are almost consistent (Fig. 5d and Supporting Informaition Table S4). H&E and STING immunohistochemical staining showed aspirin-treated group indeed had lower inflammatory cells and STING expression (Fig. 6a). Lung lesion uptake values (%ID/g) derived from PET quantitative analysis have strong correlations with H&E score ($r^2 = 0.7133$) and STING immunohistochemical staining score ($r^2 = 0.9325$), respectively (Fig. 6b and c). Fig. 6d shows the frequency and number of macrophages and neutrophils in the lungs of ALI mice treated with aspirin were decreased, when compared with those treated with saline ($^{***}P < 0.001$ and $^{**}P < 0.01$). Besides, the STING expression in macrophages and neutrophils also dropped down with aspirin treatment ($^{**}P < 0.01$ and $^{**}P < 0.01$, respectively, Fig. 6e). There is no significant difference in the frequency and number of $STING^+$ DC, $STING^+$ $CD8^+$ $CD3^+$ T cells and $STING^+$ $CD4^+$ $CD3^+$ T cells between saline-treated and

Table 1 [^{18}F]FBTA uptake (%ID/g) and CT House field (HU) value in the lungs of mice. $P > 0.05$ (ns), $^{*}P < 0.05$ and $^{***}P < 0.001$.

Probe	Group	%ID/g	*P*	-HU	*P*
[^{18}F]FBTA	1: Saline	0.33 ± 0.07	[1,2], $^{***}P$	336.14 ± 11.50	[1,2], ns
	2: LPS-2 h	2.89 ± 0.38	[1,3], $^{***}P$	328.79 ± 14.79	[1,3], $^{***}P$
	3: LPS-12 h	7.92 ± 0.24	[1,4], $^{***}P$	155.30 ± 28.38	[1,4], $^{***}P$
	4: LPS-24 h	15.96 ± 0.62	[2,3], $^{***}P$	63.33 ± 26.15	[2,3], $^{***}P$
			[2,4], $^{***}P$		[2,4], $^{***}P$
			[3,4], $^{***}P$		[3,4], $^{*}P$
[^{18}F]FDG	5: LPS-24 h	5.82 ± 1.59	[4,5], $^{***}P$	87.94 ± 9.89	
[^{18}F]FBTA	6: Saline-treated	5.16 ± 0.10	[6,7], $^{***}P$	75.29 ± 5.68	[6,7], $^{***}P$
	7: Aspirin-treated	0.65 ± 0.05		327.16 ± 42.13	

aspirin-treated groups (Supporting Informaition Fig. S15a, b). Collectively, the above data show that [^{18}F]FBTA-PET imaging could be applied in ALI therapeutic evaluation by targeting STING in macrophages and neutrophils.

3. Discussion

Given the crucial role of STING in ALI and the advantages of PET tracers in non-invasive detection at molecular level, it is necessary to construct a STING-targeted PET tracer for clinical alert and therapeutic evaluation of ALI. Here, a novel STING-targeted PET tracer, [^{18}F]FBTA, was labeled and evaluated in ALI mice to quantify lung inflammation. The STING-targeted strategy has been proven to be more sensitive than CT and more specific than [^{18}F]FDG. In addition, we demonstrated the potential clinical utility of the tracer by illustrating its therapeutic evaluation ability in ALI mice, which is a key step that is often omitted in many preclinical imaging studies.

The shortcomings of existing inflammatory biomarkers and corresponding tracers, such as over-expression of biomarkers in heart and bone marrow, nonspecific, insensitive, or poor metabolic kinetics, etc., prompt us to seek a new target and design a novel probe for alert and therapeutic evaluation of ALI. STING represents the activation of innate immunity and determines the severity of lung inflammation in ALI[25,26]. Compared with cellular glucose metabolism and other immune cell biomarkers, STING provides an earlier and more comprehensive picture of the immune status during ALI[25,26]. Therefore, we choose STING as a biomarker for evaluating ALI in mice and human lung inflammation tissues in this study.

The STING-targeted PET probe, [^{18}F]FBTA, was labeled with high radiochemical yield and high molar activity. The molecular skeleton of [^{18}F]FBTA is mainly based on a STING agonist-benzothiophene derivative with high STING affinity, high stability, low toxicity and can be used in both human and mice[29]. [^{18}F]FBTA exhibited good stability in saline and ethanol as well as high affinity and specificity for targeting STING in THP-1 cells. The quantitative PET results confirmed that [^{18}F]FBTA can trace ALI *in vivo* and accurately evaluate the degree of lung inflammation. The PET-derived radioactive uptake values were significantly correlated with LPS-induced time, H&E score and STING immunohistochemistry staining score, supporting the potential role of [^{18}F]FBTA in warning ALI. Moreover, [^{18}F]FBTA had been identified to be able to trace small lesions undetected by CT in the early stage of ALI. Flow cytometry data indicated that STING^{+} macrophages and STING^{+} neutrophils are the main cells for [^{18}F]FBTA uptake, supporting the important roles of these two types of cells in ALI.

The accumulation and activation of inflammatory cells in the lung during the initial phase before obvious clinical symptoms may lead to the elevation of membrane glucose transporters (GLUT), which may underlie [^{18}F]FDG accumulation at the site of inflammation[36]. However, this increased glucose metabolism is not only found in inflammatory cells, but also in other metabolically active lung parenchymal cells and pulmonary effusion, which leads to a failure to detect ALI from these high uptake areas[37,38]. All the non-specific uptakes will increase the false-positive findings of ALI diagnosis. Our experiments have shown that the distribution and specificity of [^{18}F]FBTA is superior to that of the glucose metabolism tracer [^{18}F]FDG. [^{18}F]FBTA shows relatively lower uptake in the heart (8.92 ± 0.53 %ID/g), an adjacent organ of the lung, and higher specificity in lung inflammation lesions (15.96 ± 0.62 %ID/g). On the contrary, the uptake of [^{18}F]FDG in the heart (29.50 ± 4.84 %ID/g) is extremely high, which affects the judgment of lung lesions (5.82 ± 1.59 %ID/g). [^{18}F]FBTA also exhibits better specificity than [^{18}F]FDG in tracing ALI inflammation process. Combining the above results and the reported conclusions, we believe that [^{18}F]FBTA represents a manifest improvement over [^{18}F]FDG in imaging lung inflammation.

^{67}Ga/^{68}Ga-citrate[20,21], ^{64}Cu-αCD11b[22], ^{64}Cu-DOTA-ECL1i[23] and ^{64}Cu-LLP2A[24] can target specific receptors or proteins of immune cells and dynamically reflect the spatial distribution of immune cell-mediated inflammation in ALI. However, the high uptake in organs or tissues of no interest and poor metabolic kinetics of these tracers affect the judgment of lung injury lesions[20−24]. Here, we compare in detail the differences in imaging parameters and distributions between the above tracers and [^{18}F]FBTA. Specifically, ^{67}Ga/^{68}Ga-citrate is mainly distributed in the heart, liver and blood, and lacks specificity as an inflammation imaging tracer[20,21]. The uptake of ^{64}Cu-αCD11b, ^{64}Cu-DOTA-ECL1i and ^{64}Cu-LLP2A in the lungs of ALI group was 3.1, 4.5 and 1.5 times than that of the control group, respectively, while the ratio of [^{18}F]FBTA in the lungs of the ALI group and control group reached 48.4 times. In addition, these ^{64}Cu-labeled antibodies or polypeptides also have a high non-specific uptake in liver[22−24], while the uptake of [^{18}F]FBTA in the liver is relatively low. ^{64}Cu-αCD11b also has a high non-specific uptake in bones[22], whereas no significant bone uptake was found in the other probes. Last but not least, the time interval between injection and imaging of all ^{64}Cu-labeled probes mentioned above is up to 24 h, while the time interval of [^{18}F]FBTA is only 0.5−1 h. Obviously, a long time interval between injection and imaging is detrimental to the diagnosis of patients with acute inflammation, thus limiting the clinical translation and application of these probes. However, whether ventilator-induced lung injury can be detected by [^{18}F]FBTA is unknown and needs to be confirmed by further studies.

ALI is a common important cause of morbidity and mortality in critical patients[2−4]. In addition, those who survive often suffer permanent lung damage, resulting in reduced quality of life, functional dependence and impairment[8,39]. Preventive drug intervention programs, based on alert diagnosis, have been proven to be effective in preventing lung inflammation of ALI in clinical trials and significantly improve prognosis in patients[7,14,40]. However, the inadequacy of current therapeutic evaluation methods has resulted in limited preventive treatment strategies, and only a few drugs have been proven to be effective. Our STING-targeted strategy confirmed that aspirin can effectively reduce inflammation to protect the lungs by eliminating immune cells, such as macrophages and neutrophils. As demonstrated here, STING-targeted [^{18}F]FBTA-PET imaging can provide insights into these temporal and spatial dynamics *in vivo*, which may aid in therapeutic monitoring and facilitate drug development.

4. Conclusions

In conclusion, a novel ^{18}F-labeled STING-targeted radiotracer, [^{18}F]FBTA, has been labeled with high yield and high molar activity. We preliminary prove [^{18}F]FBTA is a useful tool for pre-

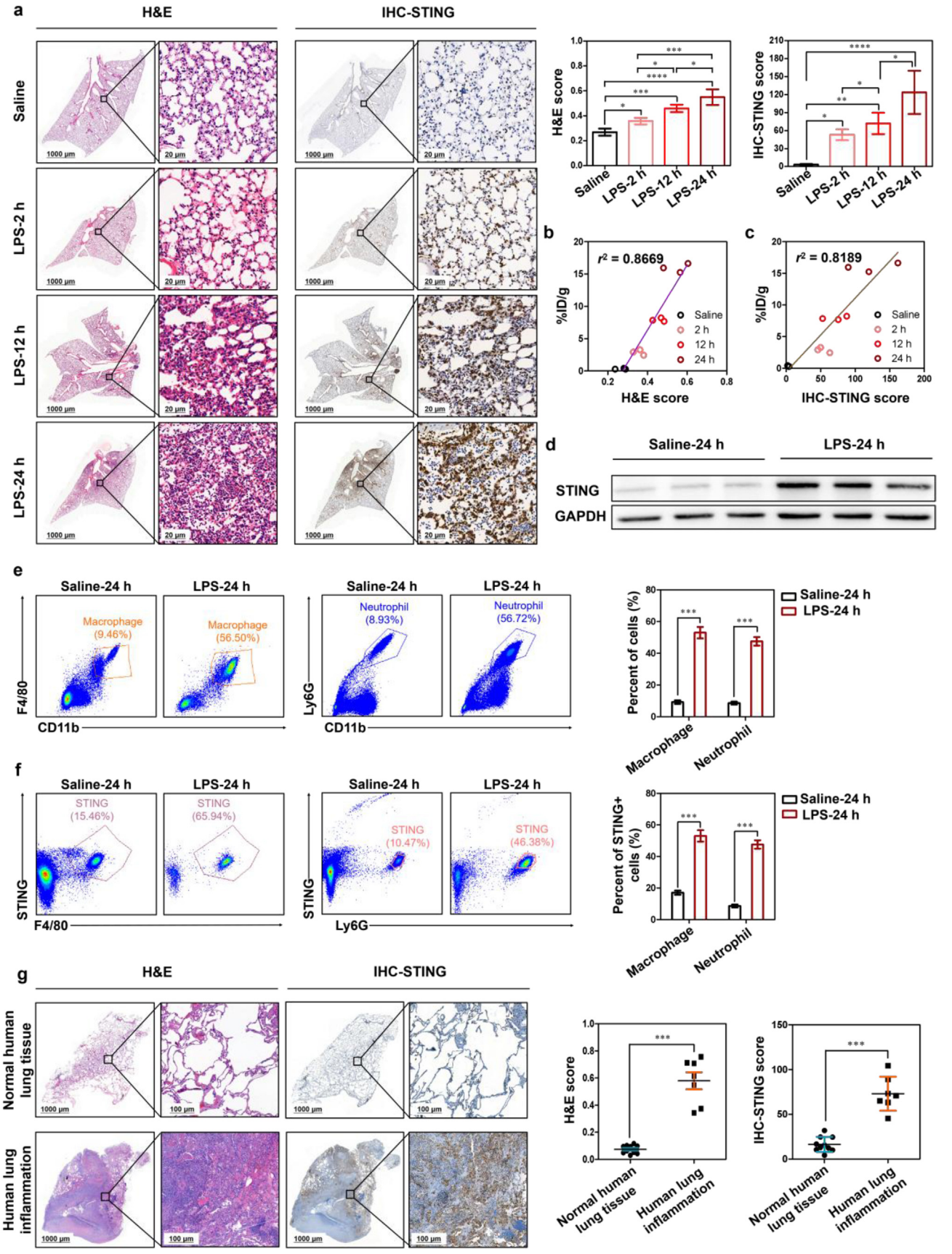
a
H&E
IHC-STING
Saline
LPS-2 h
LPS-12 h
LPS-24 h
1000 μm
20 μm
H&E score
IHC-STING score
b
c
r² = 0.8669
r² = 0.8189
%ID/g
Saline
2 h
12 h
24 h
d
Saline-24 h
LPS-24 h
STING
GAPDH
e
Macrophage (9.46%)
Macrophage (56.50%)
Neutrophil (8.93%)
Neutrophil (56.72%)
F4/80
CD11b
Ly6G
Percent of cells (%)
Macrophage
Neutrophil
f
STING (15.46%)
STING (65.94%)
STING (10.47%)
STING (46.38%)
Percent of STING+ cells (%)
g
Normal human lung tissue
Human lung inflammation
100 μm

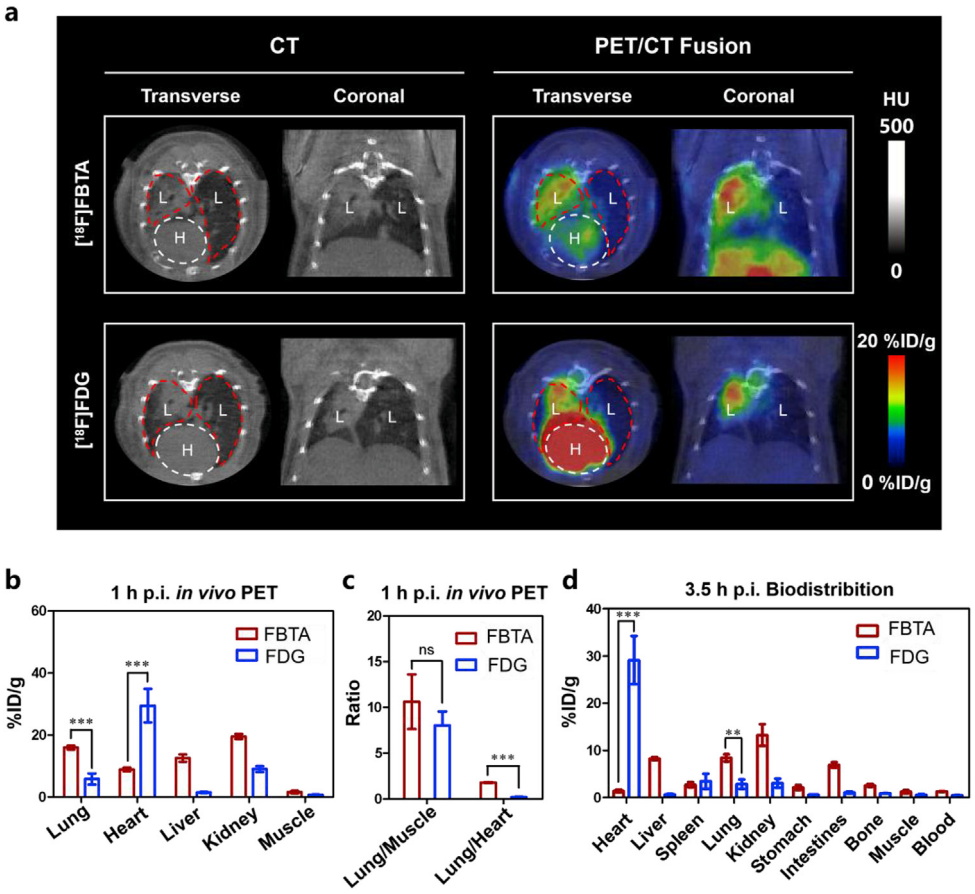

Figure 4 Comparison of [^{18}F]FBTA-PET and [^{18}F]FDG-PET imaging in ALI mice. (a) Transverse and coronal PET/CT images of [^{18}F]FBTA (11.1−14.8 MBq) and [^{18}F]FDG (14.8 MBq) in ALI mice. The lungs are indicated by red lines and hearts are indicated by white lines. L presents lung and H presents heart. (b) Quantification of [^{18}F]FBTA and [^{18}F]FDG accumulation in the lung, heart, liver, kidney and muscle at 1 h p.i. PET data are shown as %ID/g ± SD (n = 3). (c) Lung to muscle ratios and lung to heart ratios of [^{18}F]FBTA and [^{18}F]FDG derived from PET quantification. (d) Biodistribution data of [^{18}F]FBTA and [^{18}F]FDG in major organs and tissues at 3.5 h p.i. Data are shown as %ID/g ± SD (n = 3). $P > 0.05$ (ns), $^{**}P < 0.01$ and $^{***}P < 0.001$.

clinical alert and therapeutic evaluation of ALI, which makes it a potential candidate for clinical translation. But there are still several issues need to be further explored in this study. Firstly, further experiments will be performed to verify the feasibility for clinical PET guided alert diagnosis and therapeutic evaluation of human ALI. Secondly, given the key role of STING in the initiation of innate immunity, [^{18}F]FBTA may also provide warning signals for other diseases besides ALI, such as rheumatoid arthritis[41] and myocardial infarction[42], etc. Thirdly, in order to identify drugs for the treatment of ALI, the [^{18}F]FBTA-PET can also be used as a rapid and visual assessment tool for screening effective drugs in the future.

5. Experimental

5.1. *Reagents and instruments*

All of the reagents and materials, including [^{18}F]F$^-$ and [^{18}F]FDG, were obtained commercially. HPLC (Elysia-raytest GmbH) was equipped with an UltiMate 3000 pump (DIONEX) and a B-FC-1000 flow counter radioactivity detector (Bioscan). Hypersil GOLD-C18 reversed-phase HPLC column (250 mm × 4.6 mm, 5-μm particle size; Thermo Scientific) was used for analysis. PET imaging was performed with a nanoScan PET/CT preclinical scanner (Mediso). Radioactivity counts were

Figure 3 Tracking the expression of STING in LPS-induced ALI mice and human inflammatory lung tissues. (a) Representative H&E staining (bar: 1000 and 20 μm), STING immunohistochemistry staining (bar: 1000 and 20 μm) and its scores of control group and ALI groups (n = 3 per group). PET quantification of [^{18}F]FBTA accumulation in the lungs (%ID/g) demonstrates significant correlation with (b) H&E score (r^2 = 0.8669) and (c) STING immunohistochemistry score (r^2 = 0.8189). (d) Representative Western blot results in lungs of control group and ALI-24 h group. Flow cytometric plots and quantification of (e) macrophages and neutrophils in lungs and (f) STING expression in macrophages and neutrophils of control group and ALI-24 h group. (g) Representative H&E staining (bar: 1000 and 20 μm) and STING immunohistochemistry staining (bar: 1000 and 20 μm) of human normal lung tissues (n = 10) and inflammatory tissues (n = 7). $^{*}P < 0.05$, $^{**}P < 0.01$, $^{***}P < 0.001$ and $^{****}P < 0.0001$.

measured with a CRC-55tR radioisotope dose calibrator (Hitachi-IGC-7, CAPINTEC. Inc) and a γ-counter (WIZARD 2470-8020, Perkin-Elmer). A Pannoramic 250 Flash III digital scanner (3dhistech Kft, Budapest, Hungary) was used to obtain images of tissue sections. CytoFLEX Flow Cytometer (Beckman Coulter Life Sciences, USA) was used in flow cytometric sorting.

5.2. *Chemistry and radiochemistry*

The labeling precursor (compound **5**) was synthesized by a four-steps reaction using 2-fluoro-4-methoxybenzaldehyde as the starting material and the purity is $\geq$ 95%. Non-radioactive reference ([^{19}F]FBTA) was synthesized by a two-steps one-pot method using compound **5** as the starting material and the purity is $\geq$ 95%.

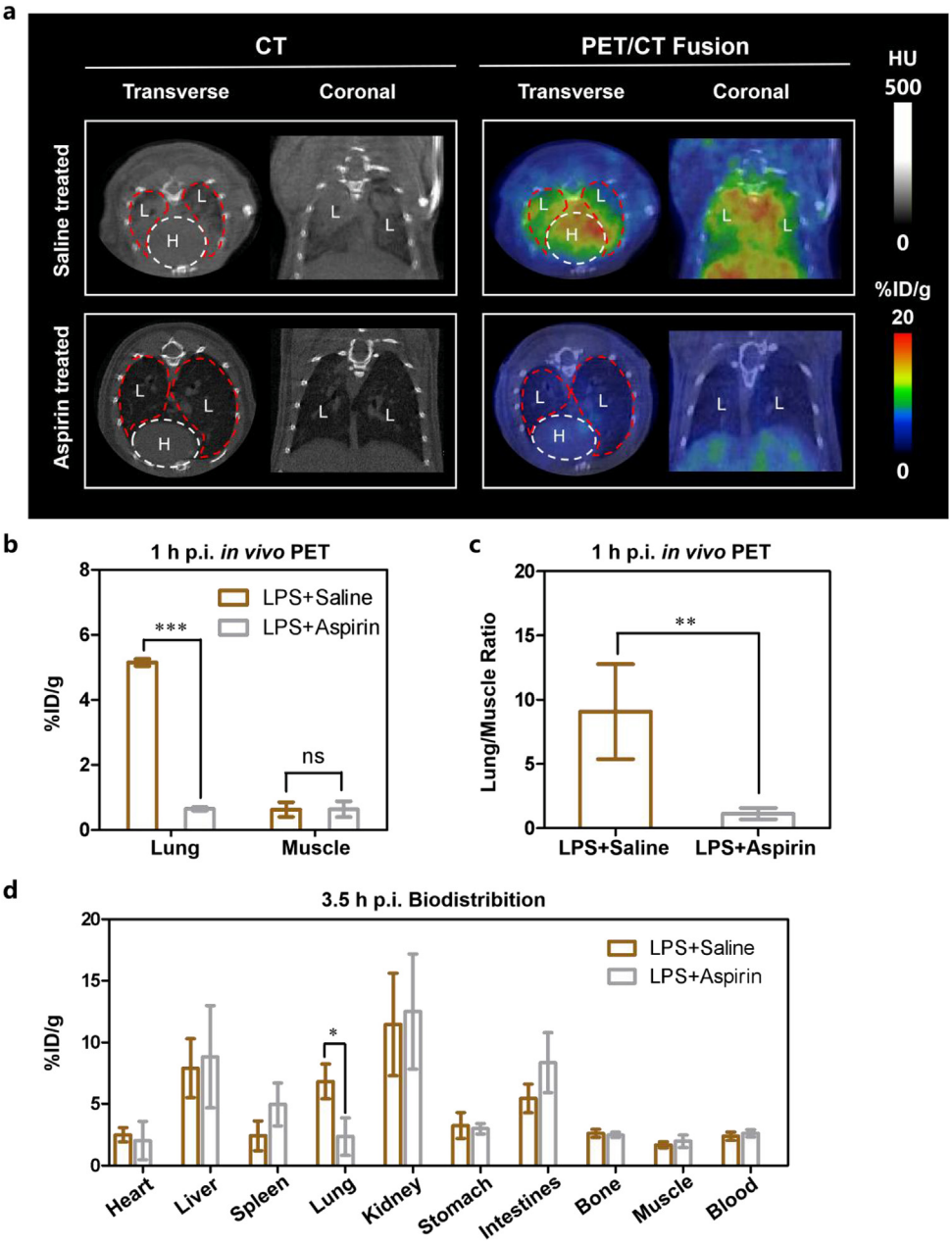

Figure 5 [^{18}F]FBTA-PET imaging, quantification and biodistribution of ALI mice in response to aspirin-treatment. (a) Transverse and coronal PET/CT images of [^{18}F]FBTA (11.1−14.8 MBq) in saline-treated and aspirin-treated ALI mice. The lungs are indicated by red lines and hearts are indicated by white lines. L presents lung and H presents heart. (b) Quantification of [^{18}F]FBTA accumulation in the lung of saline-treated and aspirin-treated ALI mice at 1 h p.i. PET data are shown as %ID/g $\pm$ SD (n = 3). (c) Lung to muscle ratios of saline-treated and aspirin-treated ALI mice derived from PET quantification. (d) Biodistribution data of [^{18}F]FBTA in major organs of saline-treated and aspirin-treated ALI mice at 3.5 h p.i. Data are shown as %ID/g $\pm$ SD (n = 3). $P > 0.05$ (ns), $^{*}P < 0.05$, $^{**}P < 0.01$ and $^{***}P < 0.001$.

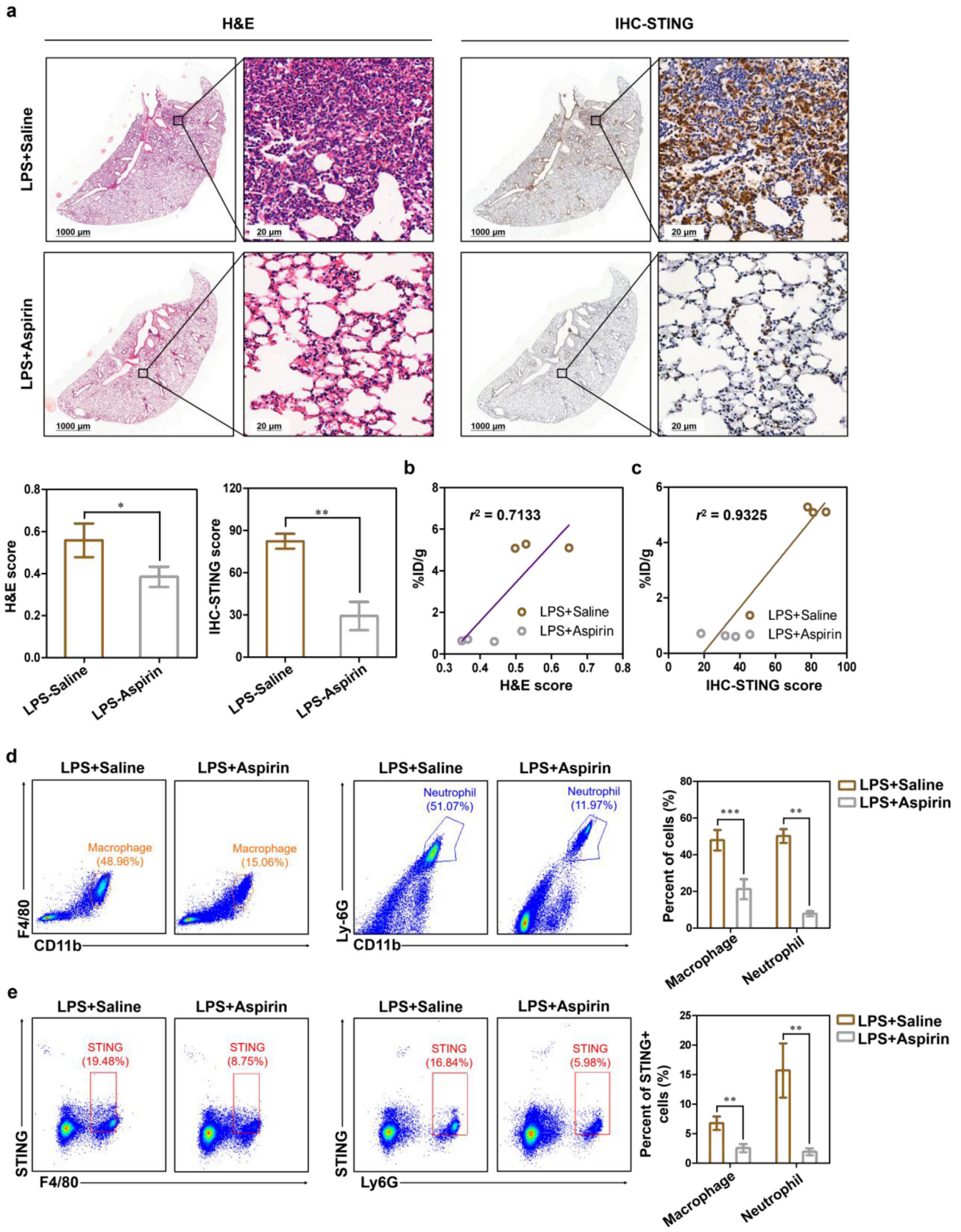

Figure 6 Tracking the expression of STING after aspirin treatment in LPS-induced ALI mice. (a) Representative H&E staining (bar: 1000 and 20 μm) and STING immunohistochemistry staining (bar: 1000 and 20 μm) of saline-treated and aspirin-treated ALI mice ($n = 3$). PET quantification of [^{18}F]FBTA accumulation in the lungs (%ID/g) demonstrates significant correlation with (b) H&E score and (c) STING immunohistochemistry score. Flow cytometric plots and quantification of (d) macrophages and neutrophils in lungs and (e) STING expression in macrophages and neutrophils of saline-treated and aspirin-treated ALI mice. *$P < 0.05$, **$P < 0.01$ and ***$P < 0.001$.

The synthesis details and methods of compounds **2**−**5** were shown in Supporting Information.

For labeling [^{18}F]FBTA, fluoride-18 was trapped on an anion exchange resin (Sep-Pak Light QMA, 20 mg, Waters) and eluted with a mixture of potassium carbonate (3 mg in 0.1 mL of deionized water) and Kryptofix[2,2,2] (14 mg in 0.1 mL of acetonitrile). QMA can trap the fluoride-18 anion and the efficiency was approximately 99%. The release efficiency of fluoride-18 anion was about 98% and a total of 1.1 GBq fluoro-18 anion would be generated to start the labeling. The eluted mixture was dried through azeotropic distillation with anhydrous acetonitrile (0.5 mL × 3) under a stream of nitrogen at 110 °C. After cooling to room temperature, 1 mg of compound **5** dissolved in 0.2 mL of anhydrous acetonitrile was added to the reaction system. The mixture was heated to 90 °C and reacted for 20 min. After cooling the mixture to room temperature, deionized water (4 mL) was added, and the mixture was passed through a Sep-Pak Plus C18 cartridge, which was then washed with deionized water (10 mL), followed by the elution of the cartridge with 1 mL of dichloromethane (DCM). Then trifluoroacetic acid (TFA, 0.5 mL) was added to the eluent (0.5 mL), reacted for 5 min at room temperature, the solvent was removed under nitrogen atmosphere at room temperature, and HPLC was used for separation and purification. The HPLC mobile phase gradient of [^{18}F]FBTA and [^{19}F]FBTA was: solvent A: water; solvent B: acetonitrile. 0 to 30 min: 35% B. Flow rate was 1 mL/min. HPLC conditions for separation, purification and quality control were the same as those for [^{18}F]FBTA and [^{19}F]FBTA analysis. The tracer radioactivity obtained after purification was 18−22 mCi and a whole radio-synthesis time was about 40 min. After collecting the product-containing eluate from HPLC, 5 mL of deionized water was added, and the diluted eluate was passed through a Sep-Pak Plus C18 cartridge, followed by the elution with 1 mL of ethanol. Finally, the ethanol solution of [^{18}F]FBTA was heated to 60 °C and blow-dried under the protection of nitrogen atmosphere for the following experiments.

5.3. *Relationship between UV area and amount of [^{19}F]FBTA loaded*

[^{19}F]FBTA was diluted to different concentrations (ranges from 1×10^{-6} to 1 mg/mL) and the UV absorption peak area of different concentrations of [^{19}F]FBTA was calculated by HPLC. The relationship between the concentration of [^{19}F]FBTA (x-axis) and the absorption peak area (y-axis) was obtained by linear analysis. According to Fig. S8, the linear equation of the HPLC UV absorbance standard curve of [^{19}F]FBTA is $y = 1729.2x+3.22$, $R^2 = 0.9996$.

5.4. *The octanol-to-water partition coefficient (logP)*

The log$P$ affects the absorption, distribution, transport, and metabolism of radiotracers. The general experimental steps were as follows: firstly, a 0.025 mol/L PBS buffer solution with pH = 7.4 was prepared. An equal volume of 1-octanol solution was added to the PBS, vortexed thoroughly, and then left to stand for more than one day. 1 mL of 1-octanol and 1 mL of PBS were added to a centrifuge tube containing 370 kBq of dried [^{18}F]FBTA. The radiotracer and the solvent were thoroughly mixed and vigorously vortexed for 5 min, followed by centrifuging at 5000 rpm for 5 min. Add 100 μL of the 1-octanol phase to a new centrifuge tube containing 0.9 mL of 1-octanol and 1 mL of PBS, and the above steps were repeated three times. Finally, 100 μL of the organic layer and 100 μL of the aqueous layer solution ($n = 3$) were taken and measured by an automatic γ-counter to calculate log$P$.

5.5. *Stability of [^{18}F]FBTA*

Two systems, physiological saline and ethanol, were selected for the study of the *in vitro* stability of [^{18}F]FBTA. To monitor the stability, a certain amount of [^{18}F]FBTA must be dissolved in physiological saline or ethanol, and incubated for 4 h at room temperature. During the incubation, the samples were analyzed by HPLC and the radiochemical purity of the compound was used to determine whether it was stable.

5.6. *STING-binding studies*

The THP-1 cells were purchased from the Type Culture Collection of the Chinese Academy of Sciences (Shanghai, China). THP-1 cells were cultured in DMEM/high-glucose medium (Gibco, Carlsbad CA, USA) containing 10% of fetal bovine serum (Gibco), 100 U/mL of penicillin, and 100 mg/mL of streptomycin (Beyotime, Shanghai, China). All cells were placed in a 37 °C incubator with a moist atmosphere of 5% of CO_2 and 95% of air.

5.6.1. *THP-1 cells saturation binding assay*

2×10^5 of THP-1 cells were added to each centrifuge tube (1.5 mL) in same volume and incubated overnight. Then the cells were centrifuged and the medium was aspirated. [^{18}F]FBTA were diluted to different concentrations (0.07−148 nmol/L) and 100 μL of diluted [^{18}F]FBTA was added to the cells. Another 200 μL of DMEM/high-glucose medium was added and incubated at 37 °C for 1 h. The medium was removed after centrifugation, the cells were washed twice with ice-cold PBS (1 mL, pH = 7.4) and centrifuged twice, respectively, to obtain medium-free cells. Radioactivity was measured using a γ-counter. Graph-Pad Prism 5 was used to calculate the B_{max} and K_d value of [^{18}F]FBTA in THP-1 cells.

5.6.2. *Cell-specific binding assay*

First, 1×10^5 of THP-1 cells were added to each centrifuge tube (1.5 mL) in same volume and incubated overnight. Then the cells were centrifuged and the medium was aspirated. [^{18}F]FBTA (0.185 MBq/0.2 mL per well) was added to the cells and the cells were incubated at 37 °C for 5, 15, 30, 60, 90 and 120 min. After incubation, cells and medium were separated by centrifugation, then cells were washed with 1 mL of PBS and centrifuged, washing and centrifugation were repeated twice. The cells were collected and the radioactivity of these cells was counted using a γ-counter. In order to determine the specificity of [^{18}F]FBTA, the STING inhibitor H-151 (10 μL per well, 1 mg/mL) was added to THP-1 cells for pre-treatment. Then the cells were incubated with [^{18}F]FBTA (0.185 MBq/0.2 mL per well) at 37 °C for 5, 15, 30, 60, 90, and 120 min, followed by repeating the PBS washing (1 mL) and centrifugation twice. These cells were finally collected and a γ-counter was used for analysis.

5.7. *Animals*

All the animals involved in the experiments were purchased from the Guangdong Medical Laboratory Animal Center, and all animal experiments strictly followed the ethics committee regulations of the Fifth Affiliated Hospital of Sun Yat-sen University (No.00137).

5.7.1. Mice with ALI

ALI was induced in male Balb/c mice aged 6−8 weeks by inhaling lipopolysaccharide (LPS, 1 mg/mL) through the trachea, and the same volume of saline was inhaled as a control. Mice induced by LPS for 2, 12 and 24 h were called as ALI-2 h group, ALI-12 h group and ALI-24 h group, respectively.

5.7.2. Aspirin treatment of ALI mice

Male BALB/c mice aged 6−8 weeks were randomly assigned to the saline-treated or aspirin-treated group. Mice in the aspirin-treated group were injected with aspirin (3.3 mg/mL, dissolved in saline, Sigma−Aldrich) intraperitoneally in advance, with a dose of 0.1 mg/g each time, injected once a day for 4 days. In the saline-treated group, the same volume of saline was injected by the same way each time. Two hours after the last injection of aspirin or saline, each mouse was inhaled with 40 μL of LPS (1 mg/mL, dissolved in saline), and administrated for PET imaging at 24 h post-induction.

5.8. Human lung tissues

Paraffin-embedded human lung tissues were provided by the First Affiliated Hospital of Sun Yat-sen University. The ethics committee of the Fifth Affiliated Hospital of Sun Yat-sen University approved these studies (K102-1). Normal lung tissues ($n = 10$) and series of lung inflammation tissues ($n = 7$) were examined. Among these inflammatory tissues, causative factors for ALI were infection ($n = 1$), pneumonia ($n = 4$), contusion ($n = 1$), and puncture ($n = 1$).

5.9. Small-animal PET/CT imaging

The saline group, ALI-2 h group, ALI-12 h group, ALI-24 h group and saline or aspirin treatment group ($n = 3$ per group) were administered with 11.1−14.8 MBq of [^{18}F]FBTA in 0.1 mL of saline/ethanol mixture (9:1) by intravenous (iv) injection, respectively. Time at which the tracer was injected relative to LPS administration was 2, 12 and 24 h, respectively. The injection was a bolus and completed within 3 s and 1-h dynamic PET scan and 10-min CT scan during tidal breathing were performed immediately after the injection. To verify the specificity of the probe, mice in ALI-12 h group were co-injected with [^{19}F]FBTA (50 μg per mouse) and [^{18}F]FBTA (11.1−14.8 MBq). PET imaging was acquired at 1 h post-injection. For comparison, another ALI-24 h group ($n = 3$ per group) was also administered with 14.8 MBq of [^{18}F]FDG in 0.1 mL of saline by iv injection and 1-h dynamic PET scan and 10-min CT scan during tidal breathing were also performed immediately after the [^{18}F]FDG injection. Before PET imaging, each mouse was weighed, anesthetized with isoflurane (1.5% isoflurane in 100% oxygen), and positioned into a PET/CT scanner bed. PET images were reconstructed by using a 3D ordered subset expectation maximization (3D-OSEM) with attenuation correction. CT images were reconstructed by using a filtered back projection. CT images were also used as a guide to draw region of interest (ROI) and three-dimensional ROI was drawn over the major organs (heart, liver, kidney), muscle and inflammatory lesions of lungs. Imaging data were acquired and analyzed with the Nucline NanoScan 3.0 software (Mediso Medical Imaging System), and expressed as percentage injected dose per gram (%ID/g). All PET images were specific frames taken 1 h after injection.

5.10. Biodistribution

After the last *in vivo* imaging scans, the mouse heart was punctured for blood collection under isoflurane anesthesia before sacrifice. Shortly thereafter, all animals were perfused through the left ventricle with 0.4% of PFA (Sigma−Aldrich, Darmstadt, Germany) in 20 mL of cold PBS. Afterward, organs were harvested and radioactivity was quantified with a γ-counter and the results are expressed as %ID/g.

5.11. Histology

Mice were sacrificed, perfused with 0.4% of PFA in 20 mL of cold PBS and rinsed in PBS to remove blood on the surface of the tissue. The clean lungs were fixed with 4% paraformaldehyde and embedded in paraffin and sectioned to 4 μm slices. The mice and human lung tissue sections were stained by hemotoxylin and eosin (H&E) and STING antibody to confirm the degree of inflammation and the expression of STING. Specifically, tissue sections were blocked with 5% BSA for 1 h at room temperature, and then incubated with primary antibody overnight at 4 °C. For H&E staining, they were stained with hematoxylin and eosin, respectively. For STING staining, STING (D2P2F) rabbit monoclonal antibody (#1346, Cell Signaling Technology) was used as the primary antibody. After immersion in PBST for 3 times, the cells were incubated with enzyme-labeled goat anti-rabbit IgG polymer for 1 h at room temperature. After immersion in PBST for 3 times, DAB chromogenic solution was added dropwise. Finally, the nuclei were counterstained in hematoxylin solution for 2 min. A Pannoramic 250 Flash III digital scanner was used to obtain images of tissue sections.

5.12. Flow cytometry

After execution, the lungs were harvested from the mice and the main bronchus were dissected. After rinsing with saline, the tissues were cut into 5 mm pieces and digested with digestion medium containing collagenase I, collagenase IV, dispase II and DNase I on a shaking bed at 37 °C for 30 min. Tissue fragments were then dissociated using a GentleMACS dissociator (Miltenyi Biotec, Germany) and filtered with a 70-mesh cell sieve. Erythrocyte lysis was performed using BD Pharm Lyse (BD Biosciences, CA, USA) and the remaining lymphocytes were centrifuged for subsequent immunostaining.

Cells were stained to assess viability with dye Aqua (Invitrogen), followed by incubation with Fc Block (BD Biosciences) to block Fc Receptor. Surface staining was performed with a comprehensive mixture of fluorochrome-conjugated surface markers includes: CD45 clone 30-F11 PE/Cyanine7 (Biolegend), CD11b clone M1/70 APC (Biolegend), CD11c clone N418 Pacific Blue (Biolegend), Ly-6C clone HK1.4 Brilliant Violet 650 (Biolegend), Ly-6G clone 1A8 APC/Fire 750 (Biolegend), F4/80 clone BM8 PE/Cyanine5 (Biolegend), CD3 clone 17A2 APC (Biolegend). After surface staining, cells were fixed in 4% paraformaldehyde and permeabilized with 0.5% Triton X100. For intracellular STING staining, cells were incubated with rabbit anti-STING antibody (19851-1-AP, Proteintech) followed by incubation with FITC conjugated goat anti-rabbit secondary antibody (ab6717, Abcam). Cells were run on a CytoFLEX Flow Cytometer and data analyses were performed using CytExpert software (Beckman Coulter Life Sciences, USA). Cell populations were differentiated using sequential gating strategy.

5.13. Western blot

Lungs were isolated from the mice and lysed with RIPA lysate containing protease inhibitor (P0013C, Beyotime) on ice for 30 min. The lysate was then centrifuged at 12,000 rpm for 5 min at 4 °C, and the concentration of proteins was measured by the BCA protein assay kit (P0010, Beyotime). 50 μg of protein was mixed with loading buffer (LT101S, EpiZyme) and heated in a metal bath at 100 °C for 10 min. After cooling on ice, the protein sample was loaded onto a 1.0 mm, 10% PAGE gel and run at 80 V for 30 min, then run at 120 V for 60 min. After the electrophoresis, the protein on the PAGE gel was transferred to the PVDF membrane (66485, BioTrace). The PVDF membrane was incubated in 5% milk at room temperature for 1 h, and then washed with TBST buffer, followed by incubation with the primary antibody STING (D2P2F) Rabbit mAb (#1346, Cell Signaling Technology) and GAPDH (#2118L, Cell Signaling Technology) at 4 °C overnight. The next day, the membrane was washed 3 times with TBST and incubated with peroxidase-conjugated Goat anti-Rabbit IgG (ZB-2301, ZSGB-BIO) for 2 h at room temperature. ECL detection reagent was added dropwise to the membrane, and the protein was finally detected with iBright Imaging Systems (Invitrogen).

5.14. Statistical analysis

Statistical analysis was performed by Student's *t*-test or one-way ANOVA analysis and $P < 0.05$ is considered a significant statistical difference between groups ($P > 0.05$ (ns), $^{*}P < 0.05$, $^{**}P < 0.01$, $^{***}P < 0.001$ and $^{****}P < 0.0001$).

Acknowledgments

This work was financially supported by the National Natural Science Foundation of China Youth Program (82202207), the Department of Science and Technology of Guangdong Province (2018B030322006, China), the Science and Technology Project Grant of Zhuhai (ZH22036201210067PWC, China), and the Scientific Research Project funded by Traditional Chinese Medicine Bureau of Guangdong Province (202106080515386340, China).

Author contributions

Dan Li, Duo Xu, Jiayao Chen, Zebo Jiang and Hong Shan conceived, designed and supervised the study. Duo Xu and Tianxing Zhu performed preparation and characterization of the probe, cellular experiments and biodistribution, Zebo Jiang, Jiayao Chen, Tianxing Zhu, Fen Wang, Yitai Xiao and Zibin Liang performed the histology, flow cytometry, Western blot and analyzed the data; Lei Bi, and Guolong Huang helped PET imaging and quantification. All authors discussed and approved the contents of the manuscript. Duo Xu, Zebo Jiang, Jiayao Chen, Tianxing Zhu and Yitai Xiao wrote and revised the paper.

Conflicts of interest

No potential conflict of interest is disclosed.

Appendix A. Supporting information

Supporting data to this article can be found online at https://doi.org/10.1016/j.apsb.2022.12.017.

References

1. Wheeler AP, Bernard GR. Acute lung injury and the acute respiratory distress syndrome: a clinical review. *Lancet* 2007;**369**:1553–64.
2. Force ADT, Ranieri VM, Rubenfeld GD, Thompson BT, Ferguson ND, Caldwell E, et al. Acute respiratory distress syndrome: the Berlin Definition. *JAMA* 2012;**307**:2526–33.
3. Bellani G, Laffey JG, Pham T, Fan E, Brochard L, Esteban A, et al. Epidemiology, patterns of care, and mortality for patients with acute respiratory distress syndrome in intensive care units in 50 countries. *JAMA* 2016;**315**:788–800.
4. Mowery NT, Terzian WTH, Nelson AC. Acute lung injury. *Curr Probl Surg* 2020;**57**:100777.
5. Gattinoni L, Chiumello D, Rossi S. COVID-19 pneumonia: ARDS or not?. *Crit Care* 2020;**24**:154.
6. Ramanathan K, Antognini D, Combes A, Paden M, Zakhary B, Ogino M, et al. Planning and provision of ECMO services for severe ARDS during the COVID-19 pandemic and other outbreaks of emerging infectious diseases. *Lancet Respir Med* 2020;**8**:518–26.
7. Hamid U, Krasnodembskaya A, Fitzgerald M, Shyamsundar M, Kissenpfennig A, Scott C, et al. Aspirin reduces lipopolysaccharide-induced pulmonary inflammation in human models of ARDS. *Thorax* 2017;**72**:971–80.
8. Matthay MA, Zemans RL, Zimmerman GA, Arabi YM, Beitler JR, Mercat A, et al. Acute respiratory distress syndrome. *Nat Rev Dis Prim* 2019;**5**:18.
9. Gattinoni L, Caironi P, Pelosi P, Goodman LR. What has computed tomography taught us about the acute respiratory distress syndrome?. *Am J Respir Crit Care Med* 2001;**164**:1701–11.
10. Bernard GR, Artigas A, Brigham KL, Carlet J, Falke K, Hudson L, et al. Report of the American-European consensus conference on ARDS: definitions, mechanisms, relevant outcomes and clinical trial coordination. The Consensus Committee. *Intensive Care Med* 1994;**20**:225–32.
11. Kor DJ, Carter RE, Park PK, Festic E, Banner-Goodspeed VM, Hinds R, et al. Effect of aspirin on development of ARDS in at-risk patients presenting to the emergency department: the LIPS-A randomized clinical trial. *JAMA* 2016;**315**:2406–14.
12. Levitt JE, Bedi H, Calfee CS, Gould MK, Matthay MA. Identification of early acute lung injury at initial evaluation in an acute care setting prior to the onset of respiratory failure. *Chest* 2009;**135**:936–43.
13. Pourfathi M, Kadlecek SJ, Chatterjee S, Rizi RR. Metabolic imaging and biological assessment: platforms to evaluate acute lung injury and inflammation. *Front Physiol* 2020;**11**:937.
14. Festic E, Carr GE, Cartin-Ceba R, Hinds RF, Banner-Goodspeed V, Bansal V, et al. Randomized clinical trial of a combination of an inhaled corticosteroid and beta agonist in patients at risk of developing the acute respiratory distress syndrome. *Crit Care Med* 2017;**45**:798–805.
15. Shaver CM, Bastarache JA. Clinical and biological heterogeneity in acute respiratory distress syndrome: direct *versus* indirect lung injury. *Clin Chest Med* 2014;**35**:639–53.
16. Han W, Zaynagetdinov R, Yull FE, Polosukhin VV, Gleaves LA, Tanjore H, et al. Molecular imaging of folate receptor β-positive macrophages during acute lung inflammation. *Am J Respir Cell Mol Biol* 2015;**53**:50–9.
17. Rodrigues RS, Bozza FA, Hanrahan CJ, Wang LM, Wu Q, Hoffman JM, et al. ^{18}F-Fluoro-2-deoxyglucose PET informs neutrophil accumulation and activation in lipopolysaccharide-induced acute lung injury. *Nucl Med Biol* 2017;**48**:52–62.
18. Tavakoli S, Short JD, Downs K, Nguyen HN, Lai Y, Zhang W, et al. Differential regulation of macrophage glucose metabolism by macrophage colony-stimulating factor and granulocyte-macrophage colony-stimulating factor: implications for ^{18}F-FDG PET imaging of vessel wall inflammation. *Radiology* 2017;**283**:87–97.
19. Pijl JP, Nienhuis PH, Kwee TC, Glaudemans A, Slart R, Gormsen LC. Limitations and pitfalls of FDG-PET/CT in infection and inflammation. *Semin Nucl Med* 2021;**51**:633–45.

20. Weiner R, Hoffer PB, Thakur ML. Lactoferrin: its role as a Ga-67-binding protein in polymorphonuclear leukocytes. *J Nucl Med* 1981;**22**:32−7.
21. Kumar V, Boddeti DK. ^{68}Ga-radiopharmaceuticals for PET imaging of infection and inflammation. *Recent Results Cancer Res* 2013;**194**:189−219.
22. Cao Q, Huang Q, Mohan C, Li C. Small-animal PET/CT imaging of local and systemic immune response using ^{64}Cu-αCD11b. *J Nucl Med* 2019;**60**:1317−24.
23. Liu Y, Gunsten SP, Sultan DH, Luehmann HP, Zhao Y, Blackwell TS, et al. PET-based imaging of chemokine receptor 2 in experimental and disease-related lung inflammation. *Radiology* 2017;**283**:758−68.
24. Haddad J, Latoche JD, Nigam S, Bellavia MC, Day KE, Zhu Q, et al. Molecular imaging of very late antigen-4 in acute lung injury. *J Nucl Med* 2021;**62**:280−6.
25. Ma R, Ortiz Serrano TP, Davis J, Prigge AD, Ridge KM. The cGAS-STING pathway: the role of self-DNA sensing in inflammatory lung disease. *Faseb J* 2020;**34**:13156−70.
26. Ning L, Wei W, Wenyang J, Rui X, Qing G. Cytosolic DNA-STING-NLRP3 axis is involved in murine acute lung injury induced by lipopolysaccharide. *Clin Transl Med* 2020;**10**:e228.
27. Kumar V. A STING to inflammation and autoimmunity. *J Leukoc Biol* 2019;**106**:171−85.
28. Kwon J, Bakhoum SF. The cytosolic DNA-sensing cGAS-STING pathway in cancer. *Cancer Discov* 2020;**10**:26−39.
29. Pan BS, Perera SA, Piesvaux JA, Presland JP, Schroeder GK, Cumming JN, et al. An orally available non-nucleotide STING agonist with antitumor activity. *Science* 2020;**369**:eaba6098.
30. Kim DW, Jeong HJ, Lim ST, Sohn MH, Katzenellenbogen JA, Chi DY. Facile nucleophilic fluorination reactions using *tert*-alcohols as a reaction medium: significantly enhanced reactivity of alkali metal fluorides and improved selectivity. *J Org Chem* 2008;**73**:957−62.
31. Cole KP, Ryan SJ, Groh JM, Miller RD. Reagent-free continuous thermal *tert*-butyl ester deprotection. *Bioorg Med Chem* 2017;**25**:6209−17.
32. Proudfoot AG, McAuley DF, Griffiths MJ, Hind M. Human models of acute lung injury. *Dis Model Mech* 2011;**4**:145−53.
33. Johnson ER, Matthay MA. Acute lung injury: epidemiology, pathogenesis, and treatment. *J Aerosol Med Pulm Drug Deliv* 2010;**23**:243−52.
34. Braune A, Hofheinz F, Bluth T, Kiss T, Wittenstein J, Scharffenberg M, et al. Comparison of static and dynamic ^{18}F-FDG PET/CT for quantification of pulmonary inflammation in acute lung injury. *J Nucl Med* 2019;**60**:1629−34.
35. Paik JY, Lee KH, Choe YS, Choi Y, Kim BT. Augmented ^{18}F-FDG uptake in activated monocytes occurs during the priming process and involves tyrosine kinases and protein kinase C. *J Nucl Med* 2004;**45**:124−8.
36. Rodrigues RS, Miller PR, Bozza FA, Marchiori E, Zimmerman GA, Hoffman JM, et al. FDG-PET in patients at risk for acute respiratory distress syndrome: a preliminary report. *Intensive Care Med* 2008;**34**:2273−8.
37. Saha D, Takahashi K, de Prost N, Winkler T, Pinilla-Vera M, Baron RM, et al. Micro-autoradiographic assessment of cell types contributing to 2-deoxy-2-[^{18}F]fluoro-D-glucose uptake during ventilator-induced and endotoxemic lung injury. *Mol Imag Biol* 2013;**15**:19−27.
38. Dittrich AS, Winkler T, Wellman T, de Prost N, Musch G, Harris RS, et al. Modeling ^{18}F-FDG kinetics during acute lung injury: experimental data and estimation errors. *PLoS One* 2012;**7**:e47588.
39. Dowdy DW, Eid MP, Dennison CR, Mendez-Tellez PA, Herridge MS, Guallar E, et al. Quality of life after acute respiratory distress syndrome: a meta-analysis. *Intensive Care Med* 2006;**32**:1115−24.
40. Humphries F, Shmuel-Galia L, Jiang Z, Wilson R, Landis P, Ng SL, et al. A diamidobenzimidazole STING agonist protects against SARS-CoV-2 infection. *Sci Immunol* 2021;**6** : eabi9002.
41. Tansakul M, Thim-Uam A, Saethang T, Makjaroen J, Wongprom B, Pisitkun T, et al. Deficiency of STING promotes collagen-specific antibody production and B cell survival in collagen-induced arthritis. *Front Immunol* 2020;**11**:1101.
42. King KR, Aguirre AD, Ye YX, Sun Y, Roh JD, Ng Jr RP, et al. IRF3 and type I interferons fuel a fatal response to myocardial infarction. *Nat Med* 2017;**23**:1481−7.